



GRB 200716C: Evidence for a Short Burst Being Lensed

Yun Wang^{1,2} , Lu-Yao Jiang^{1,2}, Cheng-Kui Li³ , Jia Ren^{4,5}, Shao-Peng Tang^{1,2} , Zi-Min Zhou⁶, Yun-Feng Liang⁶, and Yi-Zhong Fan^{1,2} 

¹ Key Laboratory of Dark Matter and Space Astronomy, Purple Mountain Observatory, Chinese Academy of Sciences, Nanjing 210034, People's Republic of China; yzfan@pmo.ac.cn

² School of Astronomy and Space Science, University of Science and Technology of China, Hefei, Anhui 230026, People's Republic of China

³ Key Laboratory of Particle Astrophysics, Institute of High Energy Physics, Chinese Academy of Sciences, 19B Yuquan Road, Beijing 100049, People's Republic of China

⁴ School of Astronomy and Space Science, Nanjing University, Nanjing 210093, People's Republic of China

⁵ Key Laboratory of Modern Astronomy and Astrophysics (Nanjing University), Ministry of Education, Nanjing, People's Republic of China

⁶ Guangxi Key Laboratory for Relativistic Astrophysics, School of Physics Science and Technology, Guangxi University, Nanning 530004, People's Republic of China

Received 2021 July 23; revised 2021 August 20; accepted 2021 August 22; published 2021 September 15

Abstract

A tiny fraction of observed gamma-ray bursts (GRBs) may be lensed. The time delays induced by the gravitational lensing are milliseconds to seconds if the point lenses are intermediate-mass black holes. The prompt emission of the lensed GRBs, in principle, should have repeated pulses with identical light curves and spectra but different fluxes and slightly offset positions. In this work, we search for such candidates within the GRBs detected by Fermi/GBM, Swift/Burst Alert Telescope, and HXMT/HE and report the identification of an attractive event GRB 200716C that consists of two pulses. Both the autocorrelation analysis and the Bayesian inference of the prompt emission light curve are in favor of the gravitational-lensing scenario. Moreover, the spectral properties of the two pulses are rather similar and follow the so-called Amati relation of short GRBs rather than long-duration bursts. The measured flux ratios between the two pulses are nearly constant in all channels, as expected from gravitational lensing. We therefore suggest that the long-duration burst GRB 200716C was a short event being lensed. The redshifted mass of the lens was estimated to be $4.25^{+2.46}_{-1.36} \times 10^5 M_{\odot}$ (90% credibility). If correct, this could point toward the existence of an intermediate-mass black hole along the line of sight of GRB 200716C.

Unified Astronomy Thesaurus concepts: [Gamma-ray bursts \(629\)](#); [Gravitational lensing \(670\)](#)

1. Introduction

Gravitational lensing takes place when the lights coming from a distant source are bent by a clump of massive matter (such as globular cluster, dark matter halo, and black hole) as they travel toward the observer. For a strong gravitational lensing, there are visible distortions such as the formation of Einstein rings, arcs, and multiple images. Gamma-ray bursts (GRBs) occurred at cosmological distances. The radiation of a tiny fraction of GRBs could be strongly lensed by the foreground objects before reaching us (Paczynski 1986, 1987; Mao 1992). Lensed GRBs should have two groups of repeated pulses with a quasi-identical shape and spectrum but different fluxes and slightly offset locations. Due to the poor angular resolution of the gamma-ray instruments, however, the small location offsets cannot possibly be reliably resolved. Fortunately, the instruments usually have a high time resolution and the gravitational-lensing-induced time delay is detectable.

In the 1990s, several methods had been proposed to identify the lensed GRBs (Wambsganss 1993; Nowak & Grossman 1994) and since then dedicated efforts have been made to search for such events in the GRB data. For instance, Li & Li (2014) studied 2700 bursts observed by Burst and Transient Source Experiment (BATSE). Hurley et al. (2019) analyzed a sample of 2301 GRBs detected by Konus-Wind. In the past decade, the Fermi/Gamma-ray Burst Monitor (GBM) data had been widely used to hunt for the lensed events (Veres et al. 2009; Davidson et al. 2011; Ahlgren & Larsson 2020). Anyhow, just null results have been reported in these works. Very recently, Paynter et al. (2021) developed a Bayesian inference-based method to identify gravitational-lensing events

and reported tentative evidence for a lensed GRB. These previous approaches can be classified into two groups. One is to analyze the autocorrelation between pulses in the same GRB and the other focuses on the cross-correlation between different GRBs. In this work we concentrate on the former and search for the lensing bursts with a large GRB database, including 3099 Fermi/GBM events, 1297 Swift/Burst Alert Telescope (BAT) events, and 311 Hard X-ray Modulation Telescope (HXMT)/HE events. GRB 200716C, one burst detected simultaneously by all three of these instruments, is found to be a promising candidate.

This Letter is organized as follows. In Section 2, we introduce the observations of GRB 200716C and perform the autocorrelation analysis of the light curves in different energy bands. In Section 3, we provide further evidence for GRB 200716C as a lensing event. In Section 4, we summarize our results with some discussion.

2. Observation and the Autocorrelation Analysis

2.1. GRB 200716C

The prompt emission of GRB 200716C was observed by multiple satellites. The Fermi GBM team reported the detection of a possible long GRB (trigger 616633066.180458/200716957) at 22:57:41 UT on 2020 July 16 (Veres et al. 2020). The GBM light curve consists of two separated pulses with a total duration $T_{90, \text{GBM}} \sim 5.3$ s in the 50–300 keV band. At the same time, Swift/BAT triggered and located GRB 200716C (trigger = 982707), and the emission in the 50–300 keV band lasted for $T_{90, \text{BAT}} = 5.44$ s (Barthelmy

et al. 2020). In addition, HXMT/HE detected GRB 200716C (trigger ID: HEB200716956) in a routine search of the data (HXMT/HE; Xue et al. 2020). The HXMT/HE light curve has a duration of $T_{90, \text{HXMT}} \sim 2.16$ s.

In this work, we adopt the time-tagged event (TTE) data of these three satellites. The Fermi/GBM data are provided by the public science support center (FSSC) of the Fermi satellite.⁷ The Swift/BAT data are available at the website.⁸ The HXMT/HE data can be conveniently applied online.⁹ Fermi/GBM has 12 sodium iodide (NaI) detectors and 2 bismuth germanate (BGO) detectors. According to the angle between each detector and the source, we use the data of two NAI detectors (n0 and n1; 8–900 keV) and one BGO detector (b0; 200–40,000 keV). The energy range of Swift/BAT is 15–350 keV. While for HXMT/HE, the deposit energy range is 100–600 keV in normal mode.

We analyze the Swift/BAT data using standard HEASOFT tools (version 6.28). The processing of the Fermi/GBM data is done with the GBM Data Tools,¹⁰ which is very convenient for user customization. For the HXMT/HE data, we use Astropy¹¹ to manipulate the event file, and extract the light curve in different filters. We take the Fermi trigger time as the zero-point and plot the light curve for each detector in different energy bands (see the upper left panel of Figure 1).

2.2. Candidate Check

Signal autocorrelation can be used to measure the time delay of temporally overlapping signals of a gravitationally lensed system. The standard autocorrelation function (ACF) is defined as

$$C(k) = \frac{\sum_{t=0}^{N-k} (I_t - \bar{I})(I_{t+k} - \bar{I})}{\sum_{t=0}^N (I_t - \bar{I})^2}. \quad (1)$$

We adopt the Savitzky–Golay filter $F(\delta t)$ to fit the ACF sequence. The values of the window length and the order of the polynomial are set to be 101 and 3, respectively. The dispersion (σ) between the ACF and the fit $F(k)$ is

$$\sigma^2 = \frac{1}{N} \sum_{j=0}^N [C(k) - F(k)]^2, \quad (2)$$

where N is the total number of bins. As usual, we identify the 3σ outliers as gravitational-lensing candidates.

We calculate the autocorrelation values of the light curves of GRB 200716C for different detectors and in multi-energy channels, and perform the Savitzky–Golay filtering. The results are shown in the right panel of Figure 1. In all cases, the autocorrelation analyses yield significance greater than 3σ , indicating that the two pulses of GRB 200716C have rather similar temporal behaviors in each channel. The maximum significance (5.08σ) holds for the Fermi/GBM-NAI (276–900 keV) data. Furthermore, the delay times are nearly the same (≈ 1.9 s). For point sources the gravitational lensing is achromatic, thus we expect that each energy channel of a lensed GRB should autocorrelate with the same time delay.

⁷ <http://fermi.gsfc.nasa.gov/ssc/data/>

⁸ <http://www.swift.ac.uk>

⁹ <http://www.hxmt.org>

¹⁰ <https://fermi.gsfc.nasa.gov/ssc/data/analysis/gbm/>

¹¹ <https://www.astropy.org/index.html>

Motivated by these facts, we suggest that GRB 200716C is a candidate lensing event.

3. Lensing Analysis

In a gravitational-lensing system, photons that travel longer distances arrive first, because a shorter path means that the light passes through a deeper gravitational potential well of the lens, where the time dilation is stronger. The source flux is lower for the photons coming relatively later than for those earlier. Consequently, for a lensed GRB there will be at least one early pulse followed by a weaker pulse. The time delay between these two pulses is determined by the mass of the gravitational lens. For lensing of a point mass, we have (Krauss & Small 1991; Mao 1992; Narayan & Wallington 1992)

$$(1 + z_l)M_l = \frac{c^3 \Delta t}{2G} \left(\frac{r - 1}{\sqrt{r}} + \ln r \right)^{-1}, \quad (3)$$

where Δt is the time delay, r is the ratio of the fluxes of the two pulses, and $(1 + z_l)M_l$ is the redshifted lens mass. With the measured Δt and r , it is straightforward to calculate the redshifted mass $(1 + z_l)M_l$.

3.1. Bayesian Inference

In order to clarify whether the two-pulse light curve is due to the lensing effect of a single pulse, Paynter et al. (2021) developed a Python package called PyGRB^{12,13} <https://github.com/JamesPaynter/PyGRB> to create light curves from either prebinned data or time-tagged photon-event data. The PyGRB was developed for the BATSE bursts. In this work we extend it to accommodate different gamma-ray instruments such as Fermi/GBM, Swift/BAT, and HXMT/HE. We use the Bayesian statistical framework to obtain the posterior distributions of the parameters. Bayesian evidence (\mathcal{Z}) is calculated for model selection and can be expressed as

$$\mathcal{Z} = \int \mathcal{L}(d|\theta) \pi(\theta) d\theta, \quad (4)$$

where θ is the model parameters, and $\pi(\theta)$ is the prior probability. For TTE data from various instruments, the photon counting obeys a Poisson process and the likelihood $\ln \mathcal{L}$ for Bayesian inference takes the form of

$$\begin{aligned} \ln \mathcal{L}(N|\theta) &= \sum_i \ln \mathcal{L}(N_i|\theta) \\ &= \sum_i N_i \ln(\delta t_i B + \delta t_i S(t_i|\theta)) \\ &\quad - (\delta t_i B + \delta t_i S(t_i|\theta)) - \log(N_i!), \end{aligned} \quad (5)$$

where N_i stands for observed photon count in each time bin, and the model-predicted photon count consists of the background count $\delta t_i B$ and the signal count $\delta t_i S(t_i|\theta)$. Note that the differences of \mathcal{Z} among models are important for our purpose. Hence, we define different signal models $S(t_i|\theta)$ to describe whether the pulses are lensed images or not. Several functions have been proposed to describe the pulse shapes (Krauss & Small 1991; Narayan & Wallington 1992; Mao 1992; Paynter et al. 2021). Here we adopt the fast-rising exponential decay (FRED) pulse light-curve model

$$S(t|\Delta, A, \tau, \xi) = A \exp \left[-\xi \left(\frac{t - \Delta}{\tau} + \frac{\tau}{t - \Delta} \right) \right], \quad (7)$$

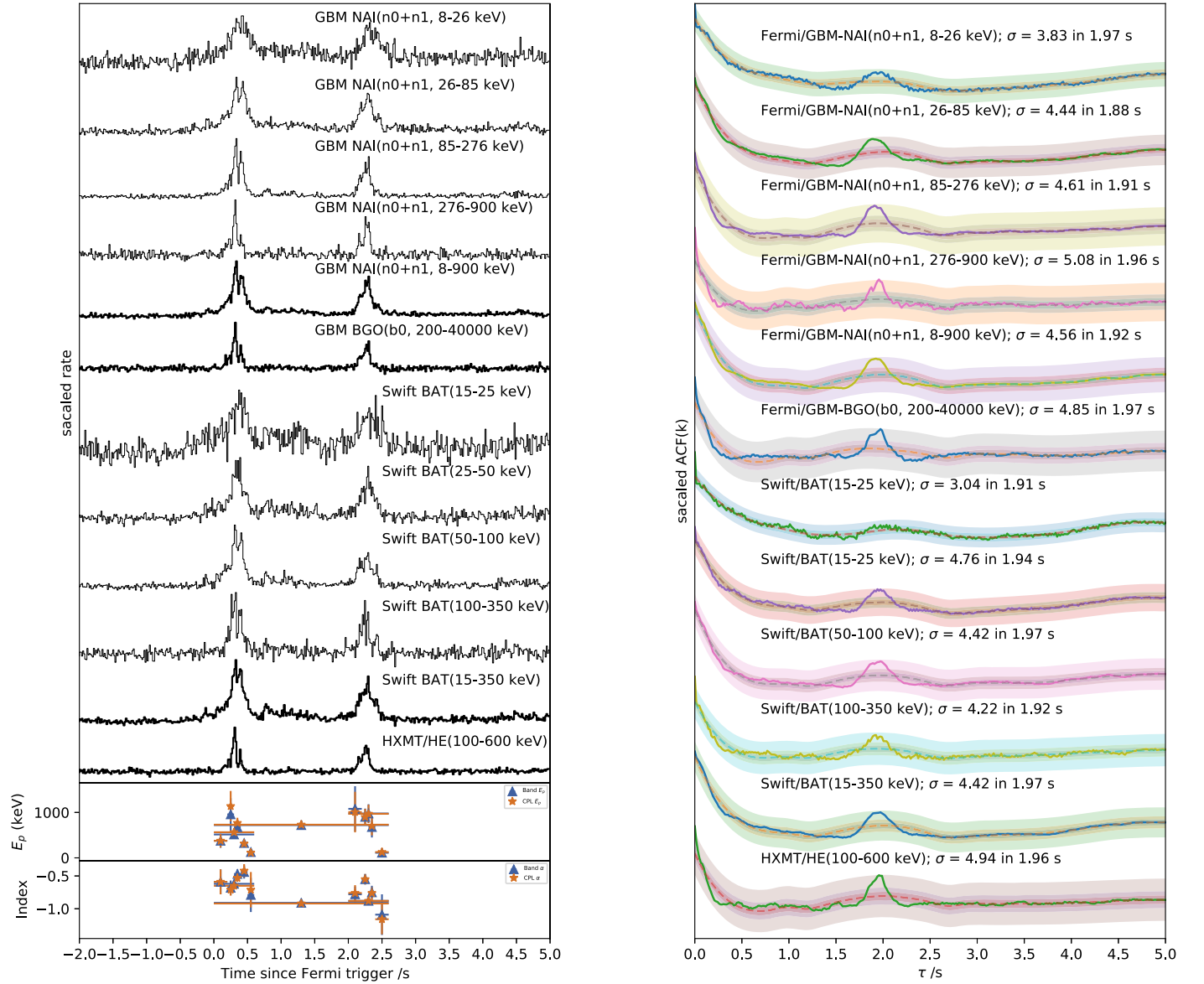


Figure 1. The upper left panel is the multi-energy band light curves of GRB 200716C observed by Fermi/GBM, Swift/BAT, and HXMT/HE. The bin size of each band is 16 ms. The middle left and lower left panels display the temporal evolution of spectral parameters E_p and α . For two pulses, the spectral parameters are similar. The right panel is for the autocorrelation results of each energy band light curve of GRB 200716C. The dashed lines in different colors represent the fits to the light curves with a 3 order Savitzky–Golay smoothing filter. The shaded regions in colors show the 1σ , 3σ , and 5σ containment bands of the Savitzky–Golay fit. The maximum significance and the corresponding time are also indicated in the plot.

where Δ is the start time of pulse, A is the amplitude factor, τ is the duration parameter of pulse, and ξ is the asymmetry parameter used to adjust the skewness of the pulse. In addition to the FRED pulses, the GRB light curve may be accompanied by a slow component (Vetere et al. 2006), which is described by a Gaussian function

$$S_{\text{gaus}}(t|\Delta, A, \sigma) = A \exp\left[-\frac{(t - \Delta)^2}{2\sigma^2}\right]. \quad (8)$$

With the above formulae, for the double pulse case (i.e., GRB 200716C) we describe the lensing and null scenarios as

$$S_{\text{lens}}(t|\theta_{\text{lens}}) = S(t|\Delta, A, \tau, \xi) + r^{-1} \cdot S(t|\Delta + \Delta_r, A, \tau, \xi) + B, \quad (9)$$

$$S_{\text{non-lens}}(t|\theta_{\text{non-lens}}) = S(t|\Delta_1, A_1, \tau_1, \xi_1) + S(t|\Delta_1 + \Delta_r, A_2, \tau_2, \xi_2) + B. \quad (10)$$

For the lensing model, r is the flux ratio between two pulses (see Equation (3)) and B is a constant background parameter. After adding a slow component, we have four models for Bayesian inference, including S_{lens} , $S_{\text{lens,gaus}}$, $S_{\text{non-lens}}$, and $S_{\text{non-lens,gaus}}$. $S_{\text{non-lens}}$ has three more parameters than S_{lens} . The influence of the number of parameters on the preference of the model, however, has been properly addressed in the calculation of \mathcal{Z} . We use the nested sampling algorithm Dynesty (Skilling 2004, 2006; Higson et al. 2019; Speagle 2020) in Bilby (Ashton et al. 2019) to sample the posterior distributions of all those parameters, typically with 500 live points. The ratio of the \mathcal{Z} for two different models is called as the Bayes factor (BF) and the logarithm of the BF

Table 1
Bayesian Inference Results

Instrument and Energy Band	$\ln \mathcal{Z}_{\text{lens}}$	$\ln \mathcal{Z}_{\text{lens,gaus}}$	$\ln \mathcal{Z}_{\text{non-lens}}$	$\ln \mathcal{Z}_{\text{non-lens,gaus}}$	$\ln(\text{BF})$	Favorite Model
Fermi/GBM-NAI						
8–26 keV	–1327.67	–1294.11	–1319.56	–1300.83	6.72	$S_{\text{lens,gaus}}$
26–85 keV	–1460.69	–1394.89	–1457.46	–1400.78	5.89	$S_{\text{lens,gaus}}$
85–276 keV	–1447.15	–1418.96	–1446.00	–1424.66	5.70	$S_{\text{lens,gaus}}$
276–900 keV	–1021.75	–1027.72	–1031.51	–1040.59	9.76	S_{lens}
Combined	–5246.53	–5120.38	–5254.53	–5166.86	46.48	$S_{\text{lens,gaus}}$
Fermi/GBM-BGO						
200–40,000 keV	–1657.76	–1661.03	–1663.07	–1666.65	5.31	S_{lens}
Swift/BAT						
5–25 keV	–1365.42	–1321.76	–1360.21	–1327.42	5.66	$S_{\text{lens,gaus}}$
25–50 keV	–1666.68	–1503.67	–1672.27	–1502.47	–1.20	$S_{\text{non-lens,gaus}}$
50–100 keV	–1740.42	–1573.11	–1735.68	–1576.34	3.23	$S_{\text{lens,gaus}}$
100–350 keV	–1419.00	–1390.37	–1419.97	–1393.90	3.53	$S_{\text{lens,gaus}}$
Combined	–6182.75	–5781.15	–6188.13	–5800.13	18.98	$S_{\text{lens,gaus}}$
HXMT/HE						
100–600 keV	–3024.81	–3023.93	–3024.84	–3024.60	0.67	$S_{\text{lens,gaus}}$

Note. The results of Bayesian inference of different models (S_{lens} , $S_{\text{lens,gaus}}$, $S_{\text{non-lens}}$, $S_{\text{non-lens,gaus}}$). By comparing the $\ln \mathcal{Z}$ given by each observation instrument with Equation (11), we get the BF ($\ln(\text{BF})$) of the lensing model versus the nonlensing model, which are 46.48, 5.31, 18.98, and 0.67 for Fermi/GBM-NAI, Fermi/GBM-BGO, Swift/BAT, and HXMT/HE, respectively.

reads

$$\ln(\text{BF}) = \max(\ln \mathcal{Z}_{\text{lens}}, \ln \mathcal{Z}_{\text{lens,gaus}}) - \max(\ln \mathcal{Z}_{\text{non-lens}}, \ln \mathcal{Z}_{\text{non-lens,gaus}}), \quad (11)$$

where the symbol “max” means taking the larger number between them. As a statistically rigorous measure for model selection, if $\ln(\text{BF}) > 8$ we have the “strong evidence” in favor of one hypothesis over the other (Thrane & Talbot 2019). The results of Bayesian inference for each model with different data are summarized in Table 1.

To estimate the global significance of the candidate lensing event, following Paynter et al. (2021) we combine the \mathcal{Z} value for each channel in different detectors and calculate the false-alarm probability. The combined BFs are found to be $\ln(\text{BF})_{\text{Fermi/GBM-NAI}} = 46.48$ and $\ln(\text{BF})_{\text{Swift/BAT}} = 18.98$, respectively. We assume that the prior odds $\pi_{\text{lens}}/\pi_{\text{non-lens}}$ is equal to $1/n$, where $n \sim 3,099$ (1, 297) is the number of GRBs detected by Fermi/GBM (Swift/BAT). Then we carry out model selection based on the posterior odds,

$$\mathcal{O}_{\text{non-lens}}^{\text{lens}} = \frac{\mathcal{Z}_{\text{lens}}}{\mathcal{Z}_{\text{non-lens}}} \frac{\pi_{\text{lens}}}{\pi_{\text{non-lens}}} \quad (12)$$

$$= \frac{p_{\text{lens}}}{1 - p_{\text{lens}}} \quad (13)$$

$$= \frac{\text{BF}}{n}, \quad (14)$$

and the false-alarm probability is $1 - p_{\text{lens}} = 1/(1 + \text{BF}/n) = 1/(1 + e^{\ln(\text{BF})}/n)$, which turns out to be 2.02×10^{-17} and 7.4×10^{-6} for Fermi/GBM-NAI and Swift/BAT data, respectively. Consequently, the lensing signal is statistically significant.

With Equation (3) and the posterior distributions of Δt and r , the 90% credibility region of the redshifted mass $(1 + z_l)M_l$ is inferred to be $3.85_{-0.94}^{+1.78} \times 10^5 M_\odot$ for the Fermi/GBM-NAI data, $3.55_{-0.99}^{+2.10} \times 10^5 M_\odot$ for the Fermi/GBM-BGO data,

$4.21_{-0.68}^{+0.79} \times 10^5 M_\odot$ for the Swift/BAT data, and $5.75_{-1.22}^{+1.93} \times 10^5 M_\odot$ for the HXMT/HE data, respectively. The combination of the above redshifted mass distributions is $4.25_{-1.36}^{+2.46} \times 10^5 M_\odot$ (90% credibility).

3.2. Spectral Analysis

We perform both time-integrated and time-resolved spectral analyses for GRB 200716C. The data of Fermi/GBM and Swift/BAT are used for joint spectral fittings. Pulse 1 and pulse 2 took place in the time intervals of $[T_0, T_0 + 0.60 \text{ s}]$ and $[T_0 + 2.00 \text{ s}, T_0 + 2.60 \text{ s}]$, respectively. We further divide them into four or five slices to examine the temporal evolution of the spectra. An empirical smoothly joined broken power-law function (the so-called “Band” function; Band et al. 1993) and a cutoff power-law (CPL) function are adopted to fit the data. The Band function takes the form of

$$N(E) = \begin{cases} A \left(\frac{E}{100 \text{ keV}} \right)^\alpha \exp\left(-\frac{E}{E_0}\right) & \text{if } E < (\alpha - \beta)E_0 \\ A \left[\frac{(\alpha - \beta)E_0}{100 \text{ keV}} \right]^{(\alpha - \beta)} \exp(\beta E - \beta E_0) \left(\frac{E}{100 \text{ keV}} \right)^\beta & \text{if } E > (\alpha - \beta)E_0 \end{cases} \quad (15)$$

where A is the normalization constant, E is the energy in units of keV, α is the low-energy photon spectral index, β is the high-energy photon spectral index, and E_0 is the break energy in the spectrum. The peak energy in the νF_ν spectrum is called E_p , which is equal to $(\alpha + 2)E_0$. The CPL function is a power law with a high-energy exponential cutoff

$$N(E) = A \left(\frac{E}{100 \text{ keV}} \right)^\alpha \exp\left(-\frac{E}{E_c}\right), \quad (16)$$

where α is the power-law photon spectral index, E_c is the break energy in the spectrum, and the peak energy in the νF_ν spectrum is equal to $(\alpha + 2)E_c$.

The Bayesian information criterion (BIC; Schwarz 1978) is adopted to evaluate the goodness of model fitting. The fitting

Table 2
Spectral Analysis Results for Various Slices

Time Interval	α	Band β	E_p (keV)	PG-stat/dof	BIC	α	CPL E_p (keV)	PG-stat/dof	BIC
(s)									
Time-resolved spectra									
Pulse 1									
(0.00–0.20)	-0.59 ± 0.19	-5.87 ± 200.83	375.98 ± 155.44	337.97/409	362.06	-0.59 ± 0.19	376.13 ± 147.56	337.96/410	356.03
(0.20–0.30)	-0.68 ± 0.11	-2.13 ± 0.25	956.93 ± 356.94	318.48/409	342.57	-0.71 ± 0.09	1138.34 ± 334.47	323.53/410	341.60
(0.30–0.40)	-0.47 ± 0.07	-2.67 ± 0.40	674.49 ± 115.72	372.35/409	396.44	-0.53 ± 0.06	767.77 ± 114.52	373.50/410	391.57
(0.40–0.50)	-0.44 ± 0.10	-5.99 ± 83.10	325.72 ± 55.49	342.33/409	366.42	-0.42 ± 0.10	313.12 ± 49.83	342.12/410	360.19
(0.50–0.60)	-0.79 ± 0.26	-6.00 ± 402.22	126.22 ± 62.25	272.38/409	296.47	-0.71 ± 0.27	112.96 ± 49.34	272.00/410	290.07
Pulse 2									
(2.00–2.20)	-0.78 ± 0.12	-5.28 ± 44.61	1079.07 ± 497.45	346.11/409	370.21	-0.76 ± 0.12	1007.62 ± 446.67	346.05/410	364.13
(2.20–2.30)	-0.55 ± 0.08	-5.90 ± 77.74	901.38 ± 183.47	354.93/409	379.02	-0.55 ± 0.08	898.67 ± 180.31	354.91/410	372.98
(2.30–2.40)	-0.75 ± 0.10	-2.81 ± 1.29	677.90 ± 229.22	320.51/409	344.60	-0.76 ± 0.09	703.42 ± 207.07	321.00/410	339.07
(2.40–2.60)	-1.09 ± 0.31	-2.61 ± 1.50	112.11 ± 94.75	393.96/409	418.05	-1.16 ± 0.23	127.51 ± 77.91	393.87/410	411.94
Time-integrated spectra									
Pulse 1									
(0.00–0.60)	-0.62 ± 0.05	-2.51 ± 0.30	514.50 ± 69.87	382.44/409	406.53	-0.65 ± 0.05	564.17 ± 64.09	384.74/410	402.81
Pulse 2									
(2.00–2.60)	-0.88 ± 0.05	-4.42 ± 8.17	976.51 ± 204.22	354.95/409	379.05	-0.88 ± 0.05	969.44 ± 200.81	354.97/410	373.04
Total									
(0.00–2.60)	-0.91 ± 0.03	-3.33 ± 1.39	720.15 ± 99.16	349.14/409	373.23	-0.92 ± 0.03	730.34 ± 94.94	349.33/410	367.40

Note. This table summarizes the results of the energy spectrum analysis for each time interval, including the parameters of the Band function (α , β , E_p) and the CPL function (α , E_p), and the value that characterizes the goodness of fit (BIC). For the detailed meaning of each parameter, see Section 3.2. In addition, in each time slice, the goodness of fit of the CPL function is better than that of the Band function. That is why the results of the CPL function are used to calculate the energy fluence.

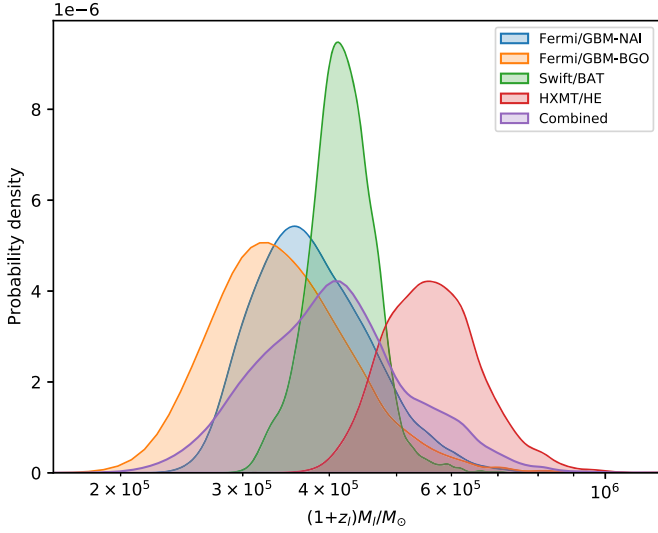


Figure 2. The redshifted lens masses inferred with different data sets. The 90% credibility region of the redshifted mass $(1+z_l)M_l$ is found to be $3.85^{+1.78}_{-0.94} \times 10^5 M_\odot$ for the Fermi/GBM-NAI data, $3.55^{+2.10}_{-0.99} \times 10^5 M_\odot$ for the Fermi/GBM-BGO data, $4.21^{+0.79}_{-0.68} \times 10^5 M_\odot$ for the Swift/BAT data, and $5.75^{+1.93}_{-1.22} \times 10^5 M_\odot$ for the HXMT/HE data, respectively. The combination of the above redshifted mass distributions is $4.25^{+2.46}_{-1.36} \times 10^5 M_\odot$.

results of different models in each time period are summarized in Table 2. Because of the low statistics of high-energy photons, β cannot be reliably constrained. By comparing the BIC values, we find that the CPL function is slightly preferred over the Band function. The temporal evolution of the spectral parameters are presented in the middle left (Band function) and lower left (CPL function) panels of Figure 1. The spectral parameters of the two pulses are similar. The evolution of the time-resolved spectral properties of pulse 1 and pulse 2 are similar, too. Such facts are in support of the gravitational-lensing model.

With the energy flux calculated by the CPL function and the possible redshift ranging from 0.384 (D’Avanzo & CIBO Collaboration 2020) to 5, we calculate the isotropic equivalent energy $E_{\gamma, \text{iso}}$ with the cosmological parameters of $H_0=69.6 \text{ km s}^{-1} \text{ Mpc}^{-1}$, $\Omega_m=0.29$, and $\Omega_\Lambda=0.71$. In panel (a) of Figure 3, we compare GRB 200716C with some other GRBs with known redshift in the so-called Amati diagram (Amati et al. 2002; Zhang et al. 2009; Yang et al. 2020). Clearly, GRB 200716C is well within the group of short GRBs, suggesting that the apparently long-duration burst GRB 200716C may be a short event being lensed.

3.3. Hardness Test

We perform a simple but statistically powerful test, i.e., the cumulative hardness comparison in different energy bands (Mukherjee & Nemiroff 2021), for the presence of gravitational lensing in GRB 200716C. This is more intuitive than energy spectrum analysis by using a parameter \mathcal{R} defined as

$$\mathcal{R} = \frac{P_{1,i} - B_i}{P_{2,i} - B_i}, \quad (17)$$

where $P_{1,i}$ and $P_{2,i}$ (B_i) represent the photon counts of the two pulses (background) over the duration in the i th energy band. We use the data from Fermi/GBM (n0) and Swift/BAT for this test, and divide them into four bands as shown in the right

panel of Figure 1. To calculate the photon counts, the time intervals of the pulses are taken to be the same as that of the spectral analysis and the background B is assumed to be a constant. The ratio errors include the Poisson noise imposed in the backgrounds as well as the pulses. Our results are presented in panel (b) of Figure 3. The resulting \mathcal{R} in different channels are nearly constant for the Fermi/GBM and Swift/BAT data, consistent with the anticipation that the lensing images should have the same hardness.

3.4. Number Density of Lenses

With Equation (29), Equation (33), Equation (34), and Equation (40) of Paynter et al. (2021), we estimate the number density of the lenses with the Fermi/GBM data set characterized by the largest number of events ($N_{\text{GRB}} = 3099$). Since the time bin of our light curves is 16 ms, we set the minimum time delay of $\Delta t_{\text{min}} = 32$ ms (the results just change a little bit for $\Delta t_{\text{min}} = 16$ ms). In the calculation of the maximum possible impact parameter y_{max} , the value of $\varphi_{\text{peak}}/\varphi_0$ is the peak photon count rate for the second most bright detector divided by the trigger threshold $kB^{1/2}$, where $k=4.5$ is the signal-to-noise ratio threshold set by the Fermi/GBM team (Meegan et al. 2009), and B is the background under Poisson statistics. Based on the current data of Fermi/GBM, we roughly estimate the median of this ratio to be 1.6 and 5.7 for peak emission timescales of 16 ms and 1024 ms, respectively. We set $z_s=(5, 2, 0.5)$ and $z_l=(2.5, 1, 0.25)$ and take $M_l = 4.25^{+2.46}_{-1.36} \times 10^5 M_\odot/(1+z_l)$. In the case of $\varphi_{\text{peak}}/\varphi_0 = 1.6$, the range of the number density of lenses is inferred to be $n_l(z_s, z_l) = (0.18-12.20) \times 10^4 \text{ Mpc}^{-3}$. While for $\varphi_{\text{peak}}/\varphi_0 = 5.7$, we have a range of $n_l(z_s, z_l) = (0.44-29.11) \times 10^3 \text{ Mpc}^{-3}$.

4. Conclusions and Discussion

In this work, we have analyzed the data of Fermi/GBM, Swift/BAT, and HXMT/HE to examine the possibility that GRB 200716C is actually a lensed short GRB. Our findings are the following:

1. The light curves of the two pulses in all energy channels are well correlated with each other, as revealed in the autocorrelation analysis as well as the Bayesian inference.
2. The temporal evolutions of the spectra of the two pulses are rather similar. In the Amati diagram, both pulses as well as the whole burst are well within the group of short GRBs.
3. The measured flux ratios between the two pulses are nearly constant in all channels.

Among the current GRB sample, such behaviors are very unusual. Intriguingly, all these facts can be straightforwardly understood in the gravitational-lensing scenario. Nevertheless, we cannot completely rule out the possibility that this event is just a very special burst consisting of two intrinsically similar pulses. If interpreted it as a lensed GRB, the redshifted mass $(1+z_l)M_l$ of the lens is about $4.25^{+2.46}_{-1.36} \times 10^5 M_\odot$ (90% credibility). For $z_l \leq 5$, the foreground object would be an intermediate-mass black hole.

Different from the previous results with the sole BATSE data, our candidate is identified with the observations from Fermi/GBM, Swift/BAT, and HXMT/HE, which cover a wider energy range and can be cross checked. We thus conclude that GRB 200716C is indeed a promising lensing

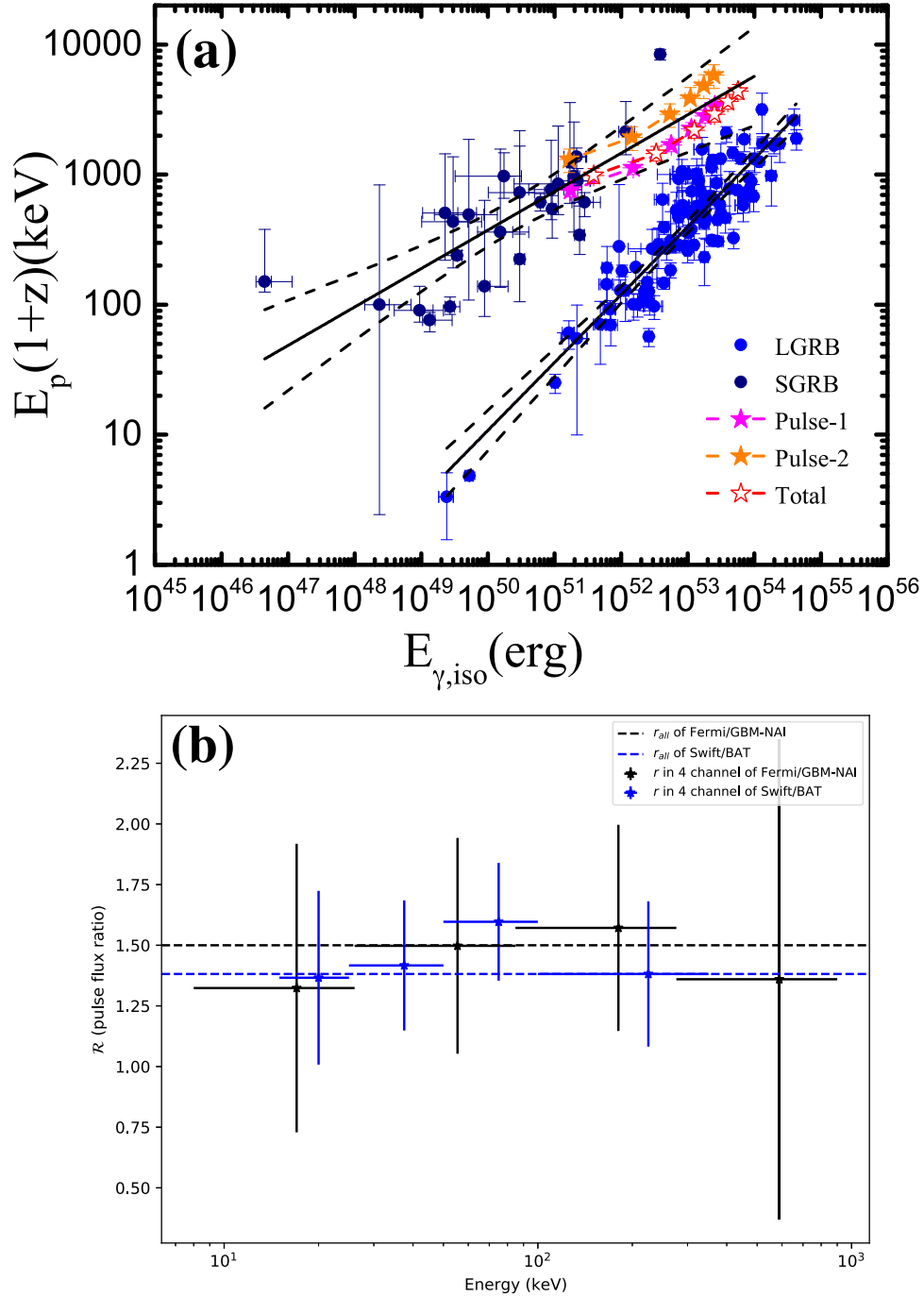


Figure 3. Two additional supports for the lensing scenario. (a) Spectral peak energy (E_p) and isotropic equivalent gamma-ray radiation energy ($E_{\gamma,iso}$) correlation diagram. The pink and orange stars represent pulse 1 and pulse 2, respectively, and the hollow red star represents the whole burst. These stars from left to right are calculated for the assumed redshifts of 0.384, 1, 2, 3, 4, and 5, respectively. Both individual pulses and the whole burst are among the short GRB group rather than the long GRB group, which is consistent with the gravitational-lensing model. (b) Cumulative hardness comparison results. For the Fermi/GBM and Swift/BAT data, the respective hardness ratios are consistent with being a constant, as anticipated in the lensing scenario.

event candidate. In this work, we focus on the specific event GRB 200716C. The analysis methods, however, can be directly applied to other sources. Our study of the large sample will be reported elsewhere.

After the submission of this Letter, the other work on GRB 200716C (Yang et al. 2021) also appeared in arXiv. In general, their analysis results are in agreement with ours except for a smaller lens mass. One reason may be that we have also included the BGO and HXMT data in the analyses, which will lead to different lens masses. These authors did not report the

uncertainty range for the derived lens mass, rendering a more careful comparison difficult.

We appreciate the anonymous referee and Dr. J. J. Wei for their helpful suggestions. We thank Dr. S. J. Lei for the kind help. We acknowledge the use of the public data from the Fermi archive, the Swift data archive, and the UK Swift Science Data Center. This work also made use of the data from the HXMT mission, a project funded by China National Space Administration (CNSA) and the Chinese Academy of Sciences

(CAS). This work is supported by NSFC under grant No. 11921003.

ORCID iDs

Yun Wang  <https://orcid.org/0000-0002-8385-7848>
 Cheng-Kui Li  <https://orcid.org/0000-0001-5798-4491>
 Shao-Peng Tang  <https://orcid.org/0000-0001-9120-7733>
 Yi-Zhong Fan  <https://orcid.org/0000-0002-8966-6911>

References

- Ahlgren, B., & Larsson, J. 2020, *ApJ*, **897**, 178
 Amati, L., Frontera, F., Tavani, M., et al. 2002, *A&A*, **390**, 81
 Ashton, G., Hübner, M., Lasky, P. D., et al. 2019, *ApJS*, **241**, 27
 Band, D., Matteson, J., Ford, L., et al. 1993, *ApJ*, **413**, 281
 Barthelmy, S. D., Cummings, J. R., Krimm, H. A., et al. 2020, GCN Circ. **28361**
 D'Avanzo, P. & CIBO Collaboration 2020, GCN Circ. **28321**
 Davidson, R., Bhat, P., & Li, G. 2011, in AIP Conf. Ser. 1358, Gamma Ray Bursts, ed. J. E. McEnery et al. (Melville, NY: AIP), **17**
 Higson, E., Handley, W., Hobson, M., & Lasenby, A. 2019, *Statistics and Computing*, **29**, 891
 Hurley, K., Tsvetkova, A., Svinkin, D., et al. 2019, *ApJ*, **871**, 121
 Krauss, L. M., & Small, T. A. 1991, *ApJ*, **378**, 22
 Li, C., & Li, L. 2014, *SCPMA*, **57**, 1592
 Mao, S. 1992, *ApJL*, **389**, L41
 Meegan, C., Lichti, G., Bhat, P., et al. 2009, *ApJ*, **702**, 791
 Mukherjee, O., & Nemiroff, R. J. 2021, *RNAAS*, **5**, 103
 Narayan, R., & Wallington, S. 1992, *ApJ*, **399**, 368
 Nowak, M. A., & Grossman, S. A. 1994, arXiv:astro-ph/9401046
 Paczynski, B. 1986, *ApJL*, **308**, L43
 Paczynski, B. 1987, *ApJL*, **317**, L51
 Paynter, J., Webster, R., & Thrane, E. 2021, *NatAs*, **5**, 560
 Schwarz, G. 1978, *AnSta*, **6**, 461
 Skilling, J. 2006, *BayAn*, **1**, 833
 Skilling, J. 2004, in AIP Conf. Proc. 735, Bayesian Inference and Maximum Entropy Methods in Science and Engineering, ed. R. Fischer et al. (Melville, NY: AIP), **395**
 Speagle, J. S. 2020, *MNRAS*, **493**, 3132
 Thrane, E., & Talbot, C. 2019, *PASA*, **36**, e010
 Veres, P., Bagoly, Z., Horvath, I., Meszaros, A., & Balazs, L. G. 2009, arXiv:0912.3928
 Veres, P., Meegan, C. & Fermi GBM Team 2020, GCN Circ. **28351**
 Vetere, L., Massaro, E., Costa, E., Soffitta, P., & Ventura, G. 2006, *A&A*, **447**, 499
 Wambsganss, J. 1993, *ApJ*, **406**, 29
 Xue, W. C., Xiao, S., Yi, Q. B., et al. 2020, GCN Circ. **28145**
 Yang, J., Chand, V., Zhang, B.-B., et al. 2020, *ApJ*, **899**, 106
 Yang, X., Lü, H.-J., Yuan, H.-Y., et al. 2021, arXiv:2107.11050
 Zhang, B., Zhang, B.-B., Virgili, F. J., et al. 2009, *ApJ*, **703**, 1696